Angelo Oliveira Silva, Dachamir Hotza, Ricardo Machado, Kurosch Rezwan, Michaela Wilhelm

+

Porous asymmetric microfiltration membranes shaped by combined alumina freeze and tape casting

Recommended Citation (primary publication/Version of Record) incl. DOI:

Angelo Oliveira Silva, Dachamir Hotza, Ricardo Machado, Kurosch Rezwan, Michaela Wilhelm,
Porous asymmetric microfiltration membranes shaped by combined alumina freeze and tape casting,
Journal of the European Ceramic Society, Volume 41, Issue 1, 2021, Pages 871-879, ISSN 0955-2219,
https://doi.org/10.1016/j.jeurceramsoc.2020.07.069

Original Article

Porous asymmetric microfiltration membranes shaped by combined alumina freeze and tape casting

Angelo Oliveira Silva[a,b], Dachamir Hotza[a], Ricardo Machado[a], Kurosch Rezwan[b,c], Michaela Wilhelm[b,*]

[a] *Federal University of Santa Catarina (UFSC), Department of Chemical Engineering (EQA), 88040-900, Florianópolis, Santa Catarina, Brazil*
[b] *University of Bremen, Advanced Ceramics, Am Biologischen Garten 2, IW3, 28359 Bremen, Germany*
[c] *MAPEX Center for Materials and Processes, University of Bremen, 28359, Bremen, Germany*

ABSTRACT

An assembled asymmetric alumina microfiltration membrane with high performance was prepared by combining freeze and tape casting techniques followed by two sintering steps. Freeze casting was used for manufacturing of the porous support layer with a highly interconnected pore network. Tape casting was applied on the top layer to form a pre-membrane with smaller pore size and controlled thickness, which was set on the sintered support. Morphology influences were investigated for different solid loadings, additives content and the assembled layer membrane structures. No delamination among the layers was observed. The assembled ceramic membrane had an average pore size between 30 and 50 μm together with a top surface layer around 0.35 μm, which is suitable to the microfiltration separation process. Porosity in the range of 26–50 % and water flux of $11–32\,m^3\,m^{-2}\,h^{-1}\,bar^{-1}$ were reached for samples prepared with two sintering steps at 1600 and 1300 °C for 2 h.

1. Introduction

Microfiltration (MF) is a well-known pressure-driven separation process, applied for concentrating, purifying or separating macromolecules, colloids and particles with a size range of $0.1-10\,\mu m$ from a suspension [1,2]. Membranes for microfiltration processes are typically made of polymers, metals, ceramics or a combination of those materials depending on costs or desired specific application [3].

Many microfiltration membranes are produced by simple technologies whereby the most suitable pore size is selected to ensure the desired separation depending on the membrane shaping and material [3]. Ceramic membranes are widely studied [4,5], and generally manufactured from alumina, zirconia, silica, mullite, perovskite, and cordierite [5,6]. In comparison to conventional polymeric membranes, ceramic membranes exhibit advantages due to their chemical and thermal stability [6,7] but still have the drawbacks of brittleness, shaping complexity and high production costs [7].

Researchers have long been interested in investigating high-performance ceramic membranes for environmental applications, desiring to improve permeability, selectivity, and reliability [8]. Controlling the ceramic membrane morphology could be a good strategy to make them very profitable and productive [9–11]. The asymmetric membrane configuration is a good strategy to improve the cost-effectiveness of the membrane [12]. Briefly, a top thin layer, or separation layer, is deposited on an intermediate layer or directly on a bottom porous support, whose pore size gradually increase from the top surface to the bottom side. Typically, an asymmetric membrane for microfiltration processes is comprised by two to three different layers [12].

Aiming a high flux, top layers generally are very thin ($< 200\,\mu m$) because the fluid mass flow through a membrane is inversely proportional to the membrane thickness. However, this decrease of thickness makes the material mechanically weak and a highly porous support to provide mechanical strength and robustness to the membranes is mandatory [13].

Ice templating, or freeze casting [14], has become a popular shaping route for all kinds of macroporous materials [15]. The possibility of a green manufacturing process avoiding the use of organic solvent and pore former together with a particular morphology, highly interconnected pore network, and controlled pore size of the samples [15,16] make freeze casting very promising to produce a macroporous support for microfiltration membrane. The process is based on freezing the solvent of a ceramic slurry and growing crystals in an emulsion, and the subsequent sublimation of the solvent. The resulting materials have been increasingly studied as macroporous support structures for many

applications like biomaterials, filtration membranes, pharmaceuticals, energy devices, among others [17–20].

Conversely, the tape casting is one of the main methods not only to produce dense, thin ceramics, and lately also for obtaining porous ceramic bodies [21]. The most common application of tape-cast structures is in the electronic industry [22,23], but nowadays their use in membrane manufacturing, especially in microfiltration became widely investigated [24–26]. The tape casting process consists of casting an appropriate ceramic slurry with the aid of a doctor blade, followed by a drying step [21].

The ceramic suspension suitable for the tape casting process contains binders and plasticizers, usually long-chain polymers, to promote pseudoplastic behavior of the slurry and suitable rigidity and flexibility of the green tape [27–29]. The casting of the ceramic suspension occurs on a flat support (normally a polymeric sheet) and the produced tape is then subjected to controlled drying in a chamber inside the tape caster [21]. The thickness of the tape is a function of the inorganic content, viscosity, casting speed and height of the doctor blade. All these parameters must be adjusted to obtain reproducible tapes. The final thickness of the tape also depends on the shrinkage that occurs during the sintering process [30].

The preparation methods of asymmetric structures may be limited to minimize the number of sintering steps but not to decrease performance. The conventional way of producing asymmetric membranes – such as pressing or extrusion for the support (flat or tubular configuration) and slip casting or dip coating of layers with smaller pore size – possess many drawbacks [31]. For example, pressed supports require organic burnout, which may lead to a non-uniform pore distribution; conversely, extrusion demands an adjustment of the rheology, which can be challenging [31]. The processing of asymmetric membranes can be further complicated by anisotropic shrinkage and cracking or delamination. All these shaping drawbacks can affect the final membrane permeability and selectivity [31].

In an asymmetric structure for microfiltration, the support is required to allow a considerable permeate flux and mechanical strength while matching the shrinkage of support and separation layer. Hence, to completely explore the advantages of high permeable supports, a more appropriate method should be employed to prepare asymmetric ceramic membranes. Taking this into account, Rachadel et al. (2017) [32] developed an innovative route for the preparation of asymmetric structures combining freeze and tape casting, by lamination of a freeze-cast support with a dense perovskite (BSCF) ceramic separation layer for oxygen permeation. Regarding microfiltration applications, it therefore seems promising to create a porous separation layer with adjusted material and porosity characteristic that can subsequently be combined with a suitable support.

This work investigates a novel application of a shaping route for porous asymmetric structures by combining tape and freeze casting. Moreover, the new approach includes a separation layer adapted to the requirements of microfiltration and to connect it with a porous support. Alumina was chosen as source material for the porous freeze-cast substrate and for the tape-cast separation layer to form asymmetric structures with the same material in order to facilitate adhesion between the layers.

Thus, this work investigates the influence of the porous support morphology on the pore size of the separation layer and the influence of the process layers on the assembled asymmetric membrane morphology. In addition, water permeability is measured to determine the effect of support and separation layer morphology on the performance of the sintered membrane for microfiltration application.

2. Experimental

2.1. Materials

The starting materials used for the membrane production were

Table 1
Overview of materials used.

Component	Function	Freeze Casting (Support), wt%	Tape Casting (Separation layer), wt%
Al$_2$O$_3$	Ceramic Powder	60−75	40−60
H$_2$O	Liquid, Solvent	25−40	40−60
Dolapix	Dispersant	1[a]	1[a]
Mowilith LDM	Binder	–	20/30[a]
PVA	Binder	1–5[a]	–
Diethanolamine	Surfactant	–	0.5[a]
Y-30	Antifoaming agent	–	0.5[a]

[a] relative to the amount of Al$_2$O$_3$.

selected according to their respective preparation process, freeze casting for the support and tape casting for the separation layer, as displayed in Table 1. Commercial alumina powder with an average particle size of 0.7 µm (CT 3000 SG, Almatis) was used as received. The solvent for both processes was deionized water (Milli Q) and the dispersant tested was a carbonic acid-based polyelectrolyte (Dolapix CE-64, Zschimmer & Schwarz). Poly(vinyl alcohol) (PVA) (Mw 20 kDa, fully hydrolyzed, Sigma-Aldrich) was used as a binder for some samples of the support layer. For the tape casting, an acrylic binder (Mowilith LDM 6138, Clariant) was used, as well as some small quantities (< 1% wt.) of surfactant (diethanolamine, Sigma-Aldrich) and anti-foaming agent (Y-30, Sigma-Aldrich).

The samples were labeled according to the forming process: Freeze Casting (FC), Tape Casting (TC) or Assembled Asymmetric Membrane (AAM). The second and third positions describe the weight percent of alumina or binder used (e.g. AAM_60A_5B1). An overview of all compounds used is shown in Table 1, whereas all samples produced from them are shown in Tab. S1

2.2. Membrane preparation

The preparation of the porous alumina support was based on non-directional freeze casting. In that case, the freezing speed was not constant and the sample froze in all directions. Briefly, alumina powder was dispersed in deionized water with 1 wt% dispersant and a total solid loading varying between 60 and 75 wt% to produce samples with varying degrees of porosity. To the sample containing 60 wt% Al$_2$O$_3$, PVA was added as a binder with 1 or 5 wt% relative to the Al$_2$O$_3$ amount. The suspension slurries were ball milled for 1 h, and then the slurry was poured into a cylindrical PTFE mold and transferred to a freezer (Sanyo MDF1155, Japan) at −150 °C for 1 h. During this step, the water froze, and the ice crystals grew to form the later pores in the micrometer scale. Subsequently, after demolding, the samples were freeze-dried for 24 h at −30 °C and 1.0 × 10^{-3} µbar for complete solvent sublimation. The green bodies were sintered at 1600 °C in air, starting at room temperature with a heating rate of 60 °C/h up to 500 °C followed for a dwell time of 1 h for debinding, and then heated up at 100 °C/h to reach 1600 °C. The dwell time at the target temperature was kept constant for 2 h. A cooling rate of 60 °C/h to 1000 °C was followed by a rate of 100 °C/h down to room temperature. The heat-treated samples were then ground and polished to obtain a disk-cylindrical structure (2 cm in diameter and 1 mm thick). The porous support was washed with water and air dried to remove residues.

The separation layers were produced using the tape-casting technique. The alumina powder was milled with water and dispersant in a planetary ball mill (Retsch PM100) at 400 rpm for 4 h using alumina beads. In the sequence, the acrylic binder (Mowilith LDM 6138, Clariant) was added to the slurry, which was further mixed in the ball mill for 30 min. The concentration of alumina powder was set at 40 and 60 wt% relative to the total slurry, while the amount of dispersant and binder was calculated considering a solid loading of 1 and 20 or 30 wt
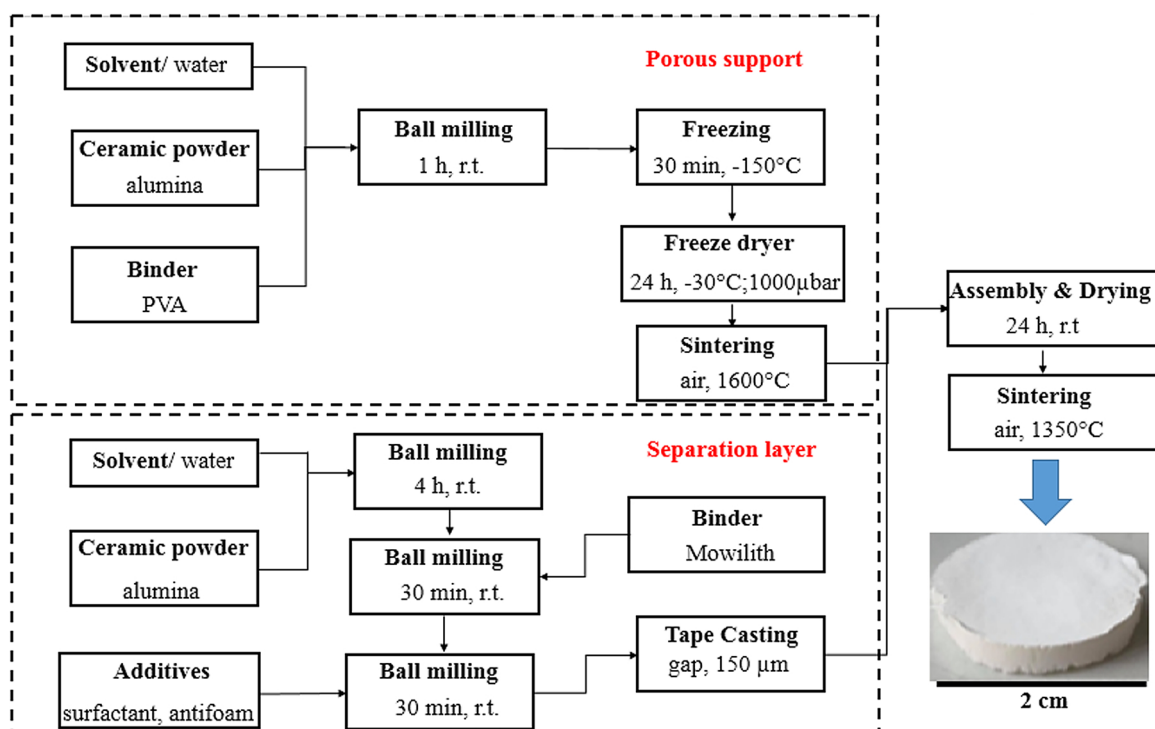
Fig. 1. Process scheme of asymmetric membrane manufacturing.

%, respectively, as presented in Table 1.

Small amounts (0.5 wt% relative to solids loading) of the anti-foaming agent (antifoam Y-30) and the surfactant (diethanolamine) were also added in the third step of milling/mixing to help to remove air bubbles from the slurry and to facilitate the removal of the cast tape after drying, respectively. Tape casting was carried out at room temperature using a manual doctor blade on a moving silicon-coated polyethylene terephthalate carrier (Mylar, G10JRM, Richard E. Mistler, Inc.). The gap between blade and carrier was adjusted to a constant value of 150 μm, and the casting speed was set on 1 mm/s.

About 30 min after casting, the pre-sintered porous carrier was placed on the partially dried tape. The assembled prepared asymmetric membranes were dried in air at room temperature for 24 h and then cut and removed from the Mylar film for the sintering step. Subsequently, the assembled asymmetric samples were thermally treated with the same heating rate and dwell times as the porous support, only changing the highest temperature to 1350 °C. All preparation steps of the membranes are illustrated in Fig. 1.

2.3. Characterization

The microstructure of the single porous freeze-cast support, single tape-cast separation layer and assembled asymmetric membranes were analyzed by Scanning Electron Microscopy (SEM, 20 kV; Series 2, Obducat CamScan; Supra 40-Carl Zeiss). For this purpose, the samples were sputtered with gold (K550, Emitech, Judges Scientific). To evaluate the pore sizes observed on the top surface and morphologies in the cross-sectional view of the single structures and sintered membranes top surface, SEM images were processed and analyzed by an image processing software (ImageJ). The number of pores detected from the SEM images varied from around 500 up to 700 data points. Tukey's mean separation test was applied as a statistical analysis for the average mean of the structures.

Open porosity and pore size distribution of the tapes, freeze-cast and assembled composite structures were determined using mercury intrusion porosimetry (Pascal 140/440, Porotec). The shrinkage of the porous support during sintering was calculated considering the sample diameter dimension before and after the heat treatment.

Specific surface area (SSA) was determined by nitrogen adsorption and desorption isotherms measured at 77 K (Belsorp-Mini, Bel Japan) and calculated according Brunauer-Emmet-Teller (BET). The samples were degassed at 120 °C for 3 h prior to measurement. Small pieces of sample were taken for the measurements.

Water permeation tests were performed using a homemade setup in a dead-end configuration (Fig. S3). The membranes were cut into a circular shape (diameter: 1 cm) and tested in triplicate at 0.5, 1.0 and 2.0 bar, which are relevant for microfiltration processes. The structures of FC and TC samples present a relatively symmetric structure, so that the membrane sides were not distinguishable. AAM samples were measured with the separation layer in contact with the water reservoir. The permeation flux was calculated according to the Eq. (1):

$$J = 1/A \ (dV/dt) \tag{1}$$

where J is the membrane permeation flux ($m^3 m^{-2} h^{-1}$); A is the effective transverse area of the ceramic membrane (m^2); dV and dt represent the variation in volume (m^3) and time (h), respectively.

3. Results and discussion

3.1. Microstructure analysis

The morphologies of sintered (a) tape-cast alumina separation layer, (b) freeze-cast alumina porous support, (c) and (d) assembled asymmetric membranes were analyzed through SEM micrographs (Fig. 2). The pore structure characteristics of single tape-cast material show an average pore size around 0.27 μm determined by ImageJ, which is suitable for microfiltration. The porous freeze-cast support exhibited a highly interconnected pore network with lamellar structured pores larger than 10 μm, which are typical for water-based freeze casting [20].

The micrographs of the assembled asymmetric membranes show two defined structures (skin separation layer on the right and porous support on the left) in the two different porous support used but in the same separation layer. Delamination of the separation layer or crack
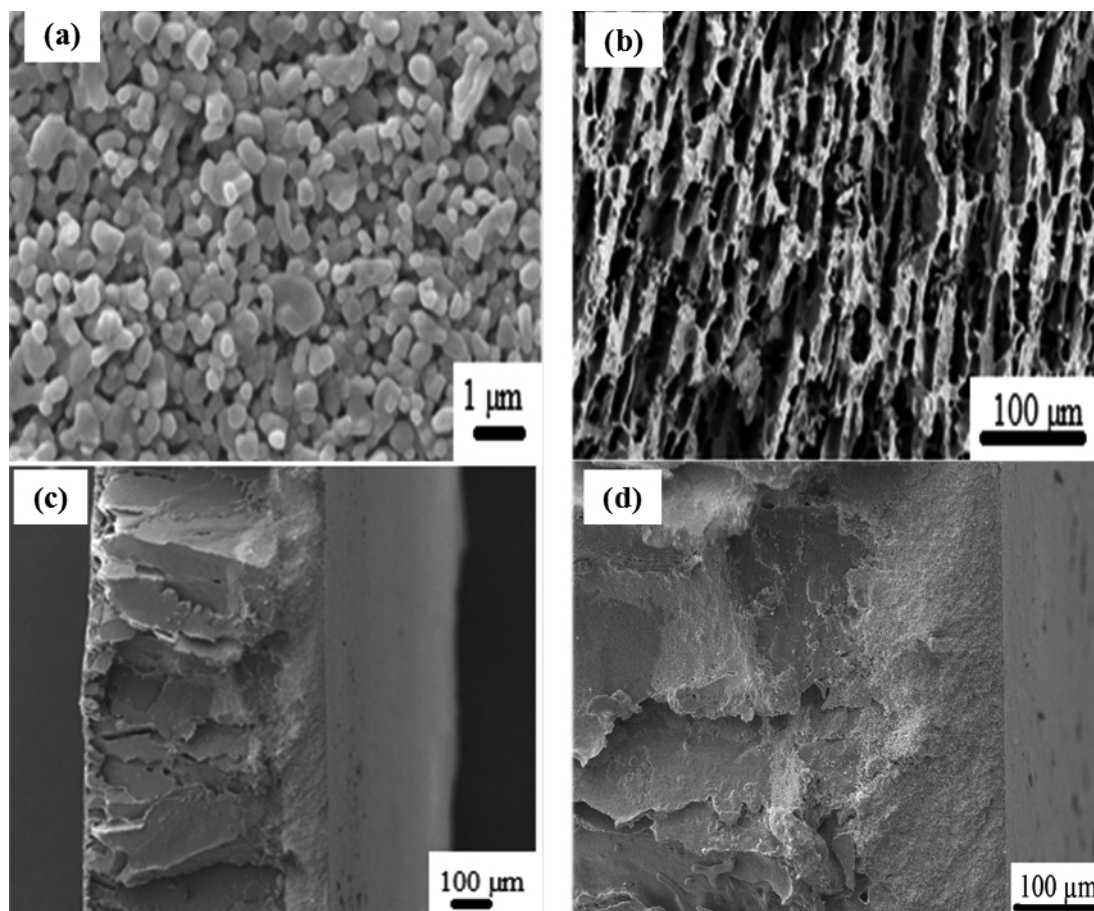
Fig. 2. Typical SEM micrographs: (a) Top view of the tape-cast layer for sample TC_60A_30B$_2$ sintered at 1350 °C; (b) Cross-sectional view of porous support material of the sample FC_60A_5B$_1$ sintered at 1600 °C; (c) and (d) longitudinal cross-sections of assembled asymmetric membranes AAM_60A_5B$_1$ sintered at 1350 °C in two different magnifications; 13500×, 40000×.

formation were not observed for the assembled asymmetric membranes.

3.2. Pore structure of separation layer

The pore size distribution of single and assembled membrane was investigated by ImageJ analysis of SEM micrographs shown in Fig. 2a (TC_60A_30B$_2$) and in Fig. S.1. The resulting average pore sizes are summarized in Table 2. The mean average pore sizes of the same separation layer on different support structures of the assembled asymmetric membranes are similar ($0.31 - 0.37\,\mu m$) and within the desired range of microfiltration membranes [1,2]. The increase on overall average pore size was expected, since the sintering temperature of the 2nd sintering step is lower than the temperature of the 1st sintering step

Table 2
Mean pore size of the separation layer (TC_60A_30B$_2$), single and assembled analyzed from SEM pictures by ImageJ.

Sample	Mean pore size (μm)[a]
TC_60A_30B$_2$	$0.27 \pm 0.14^{\alpha}$
AAM_60A	$0.37 \pm 0.23^{\beta}$
AAM_60A_1B$_1$	$0.31 \pm 0.17^{\gamma}$
AAM_60A_5B$_1$	$0.32 \pm 0.19^{\beta\gamma}$
AAM_70A	$0.36 \pm 0.20^{\beta\gamma}$
AAM_75A	$0.35 \pm 0.26^{\beta\gamma}$

[a] Average values. Within-line values distributed with different letters (α, β, γ) are significantly different ($p < 0.05$) for Tukey's mean separation test.

used for support production, as observed by Voigt et al. (2014) [33]. The average pore size of the separation layer was only slightly changed by the support structure, but it is larger than the pore size of the individually sintered single tape-cast layer ($0.27\,\mu m$).

3.3. Pore structure of support, separation layer and assembled structures

Pore size distribution was further analyzed by mercury intrusion porosimetry, which allows to measure open porosity and average pore size. Fig. 3 presents the results for the single prepared structures: (a) single tape-cast sintered at 1350 °C; (b) single freeze-cast sample without binder sintered at 1600 °C; (c) single freeze-cast sample with binder sintered at 1600 °C; and (d) single freeze-cast sample with and without binder (two sintering steps: at 1600 °C and 1350 °C). The values of average pore size, open porosity and the shrinkage of the samples during sintering are summarized in Table 3.

The pore size distribution (Fig. 3(a)) of the separation layer sintered at 1350 °C is not strongly affected by the solid loadings tested, showing an average pore size around $0.20\,\mu m$ for all samples. This is due to the intrinsic characteristics of tape casting process, in which the solvent does not act as a pore-forming agent [25]. The pore size values are similar to those estimated with ImageJ for the single separation layer TC_60A_30B$_2$ ($0.27\,\mu m$).

For the cast tapes, the open porosity is more related to the type and amount of the binder. In this case, 45.4 % was the highest open porosity with a lower number of smaller pores for TC_60A_30B$_2$. Therefore, this separation layer has been chosen for the preparation of the assembled asymmetric membrane.
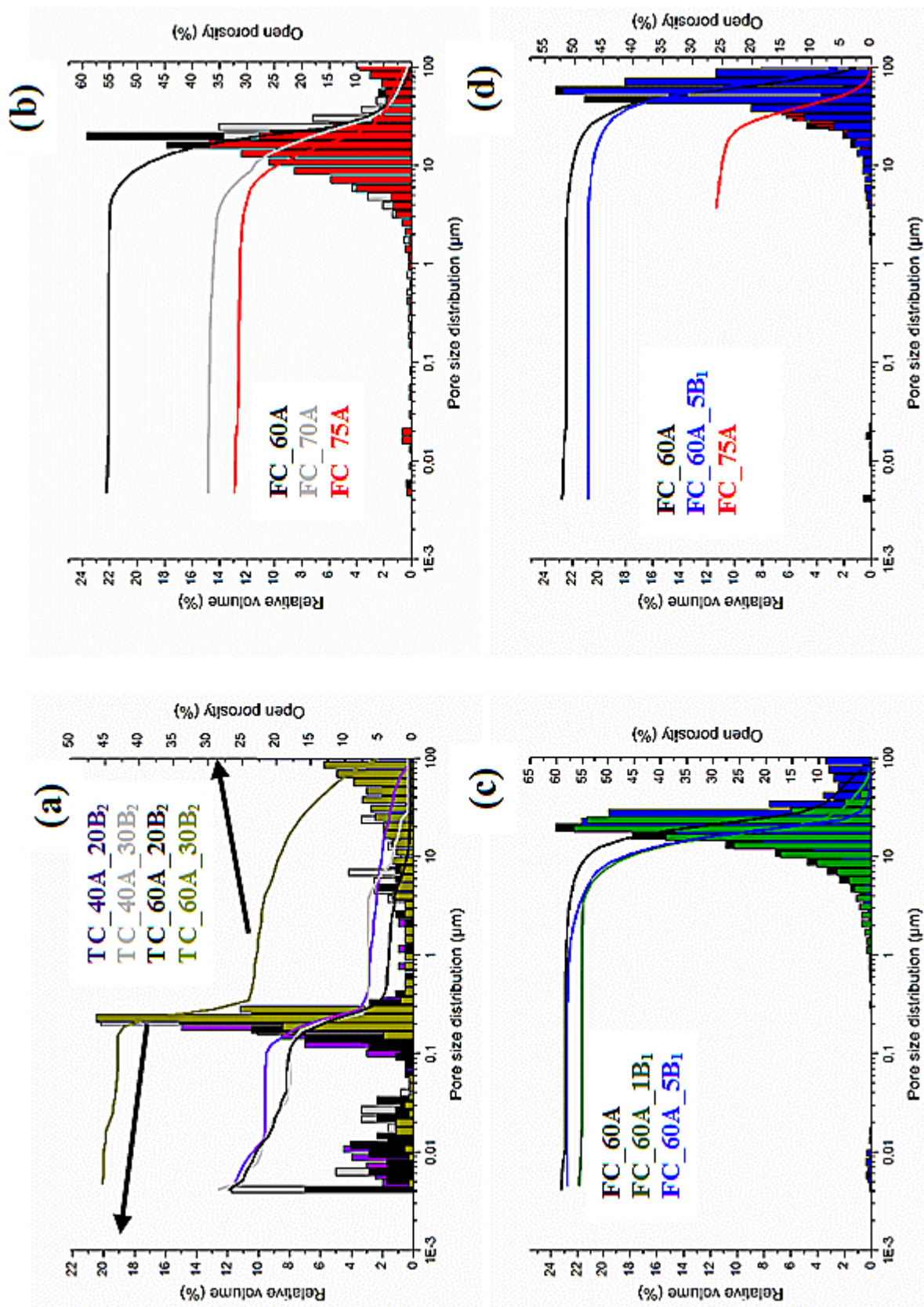
Fig. 3. Pore size distributions and open porosity of: (a) single tape-cast layers with different solid loading and binder content (sintered at 1600 °C); (b) single porous freeze-cast support with different solid loading (sintered at 1600 °C); (c) single porous freeze-cast support with different binder contents (sintered at 1600 °C); (d) single freeze-cast porous support with different solid loading and binder content (two sintering steps: 1600 °C and 1350 °C).

Table 3

Open porosity and average pore size obtained from mercury intrusion as well as shrinkage after sintering.

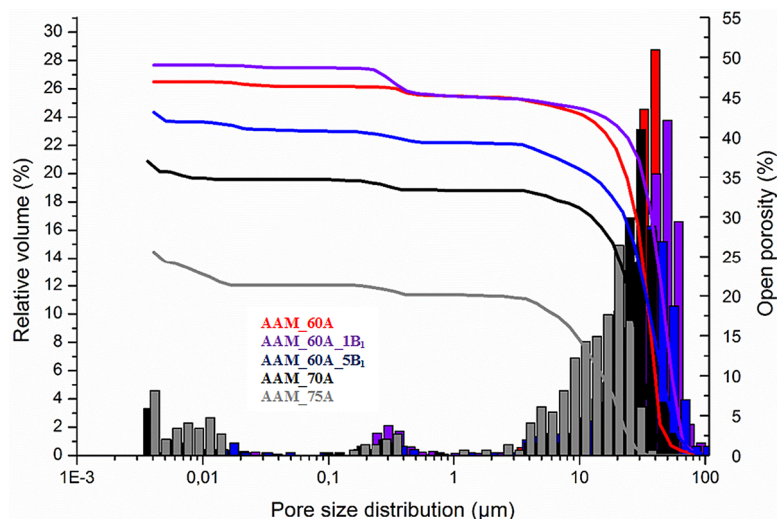| Sample	Characteristics	Open Porosity (%)	Average Pore Size (µm)	Shrinkage (%)[a]
TC_40A_20B$_2$	Single Tape Layer	26.1	0.2	
TC_40A_30B$_2$	Single Tape Layer	30.1	0.2	
TC_60A_20B$_2$	Single Tape Layer	28.0	0.2	
TC_60A_30B$_2$	Single Tape Layer	45.4	0.2	
FC_60A	Single Freeze Layer	55.7	19.7	17
FC_70A	Single Freeze Layer	30.1	24.4	
FC_75A	Single Freeze Layer	28.0	16.1	15
FC_60A_1B$_1$	Single Freeze Layer	59.1	24.9	
FC_60A_5B$_1$	Single Freeze Layer	57.9	19.0	17
FC_60A	Freeze Layer (two sintering steps)	52.4	57.4	0.1
FC_60A_5B$_1$	Freeze Layer (two sintering steps)	47.7	57.0	0.4
FC_75A	Freeze Layer (two sintering steps)	26.0	37.9	0.1
AAM_60A	Assembled Structure	46.9	39.8	
AAM_70A	Assembled Structure	37.4	34.1	
AAM_75A	Assembled Structure	26.2	37.0	
AAM_60A_1B$_1$	Assembled Structure	49.7	49.3	
AAM_60A_5B$_1$	Assembled Structure	43.7	37.0	

[a] Blank spaces were not measured.

Fig. 4. Pore size distributions and open porosity of the assembled asymmetric membranes with different solid loading and binder content.

In contrast to the pore generation mechanism in tape casting, in freeze casting the solvent is mainly responsible of the pore morphology, size and amount [15]. Fig. 3(b–c) and Table 3 present the results for the freeze-cast samples after the first sintering step at 1600 °C. Here it can be seen that the open porosity of the system decreases as the solid loading increases, because the open porosity is related to the volume of solvent released. The binder content does not show a significant impact on the open porosity, which reached values of 55.7–59.1 % at the binder conditions tested. Despite the influence on the open porosity, the pore size distribution does not seem to be strongly influenced by the solid load or binder quantity. A greater influence on the average pore size is likely to be exerted by the type of solvent and the freezing rate or temperature [34], which have been kept constant in this work.

The analysis of the single porous freeze-cast support sintered two times, at first at 1600 °C and secondly at 1350 °C (Fig. 3 (d)), shows that the pore size distribution of the support is strongly affected by the second sintering step, which promotes a significant increase in the overall pore size. However, during the second sintering step, the shrinkage values were only 0.1 − 0.4% (Table 3), so that the shrinkage is almost not affected.

An increase on average pore size was expected mainly because of the known influence of the dwell time during sintering [35,36]. The low second shrinkage indicates that the structure is already consolidated after the first heat treatment. However, when the second sintering

starts, the heat treatment promotes an increase in grain size and consequently a decrease in open porosity by 2–12 % and in the average pore size is doubled or tripled (37.9–57.4 µm). Thus, the sintering process was not complete finished after the first heat treatment.

The open porosity and pore size distribution of the support after the second sintering step are like the corresponding values of the assembled asymmetric membranes (Fig. 4 and Table 3). For this reason, double-sintered support structures were defined for evaluation of permeability in comparison to AAM membranes. However, the presence of the tape layer produces a decrease in open porosity of 4–5.5 %, and average pore size goes to 34.1–49.3 µm, except for the sample FC_75A.

The isotherms obtained from nitrogen adsorptions measurements (Fig. S.2) indicate a macroporous structure with almost no micropores. The SSA of the single tape-cast layer shows a value of 1.3 m^2/g for the tape-cast separation layer exhibiting the smallest pores. In contrast, the freeze-cast support and the assembled structures as well show SSA values of $0.1 − 0.6$ m^2/g, what confirms the absence of micropores and makes high permeabilities likely.

3.4. Permeability

The water permeate flux was measured according to the applied pressures for selected membranes and their single respective support layer after the second sintering step as shown in Fig. 5. The permeate
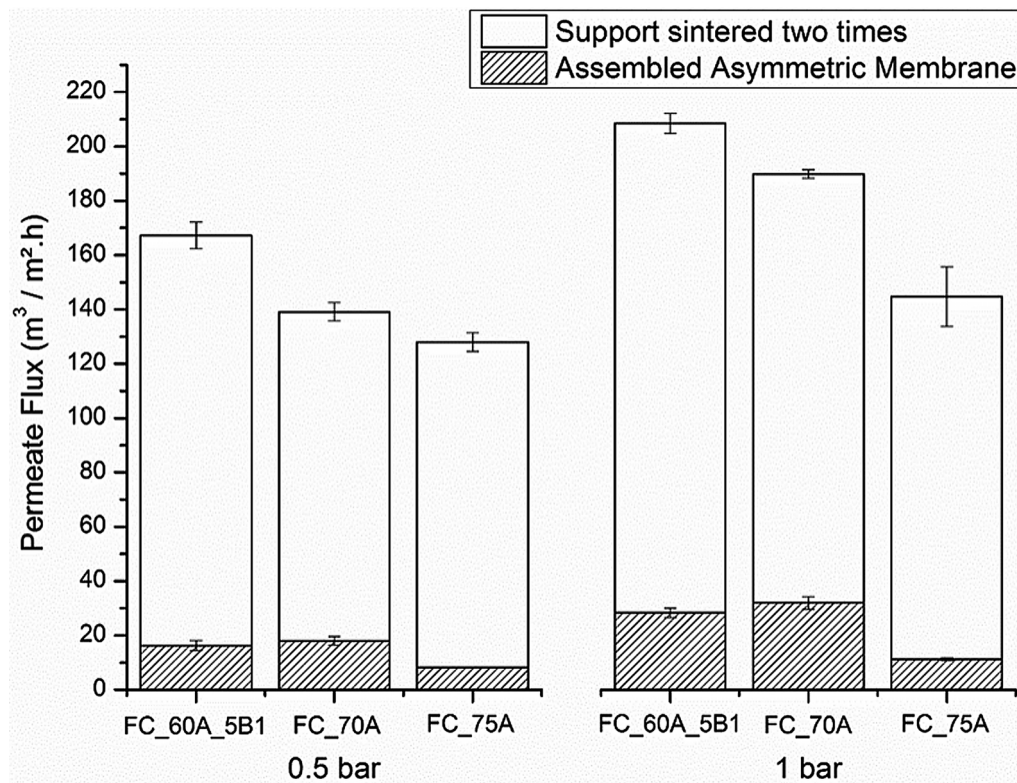
Fig. 5. Water permeate flux measured at room temperature using pressures of 0.5 and 1 bar for the porous support after two sintering steps and the assembled asymmetric membranes.
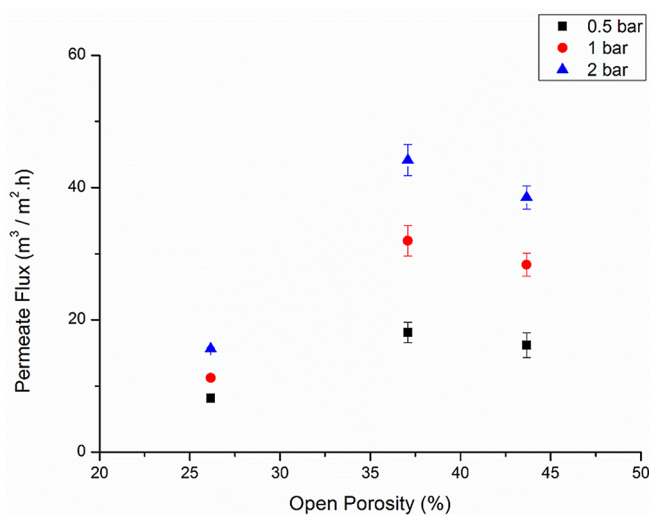

Fig. 6. Water permeate flux of the assembled asymmetric membrane AAM_75A, AAM_70A, and AAM_60A_5B₁ measured at room temperature and pressures of 0.5, 1 and 2 bar as a function of their open porosities.

flow within a membrane is a function of various parameters: open porosity, average pore size, material properties, pore cross-linking, etc. [37,38]. It is possible to distinguish differences in permeability as a function of the solid loading of the individual support. This fact is also related to the significant reduction of the permeate flux of the assembled asymmetric membrane in comparison with the individual supporting layer. It is possible to state that the separating layer acting as the functional membrane mainly determines the permeability.

A comparative analysis of the water permeate flux as a function of the open porosity of the assembled asymmetric membrane (Fig. 6) shows an approximately constant permeate flux for open porosities of 43.7 and 37.3 %, but a significant decrease in flux for sample AAM_75A (porosity < 30 %). This behavior at lower porosities shows the importance of the porosity control of the prepared membrane [38]. If the porous support does not provide sufficient porosity for the fluid liquid flow, the support starts to act as a barrier and may reduce the permeability of the system.

In Table 4, the performances of some alumina membranes suitable for microfiltration with water flux at 1 bar of transmembrane pressure are summarized. Comparing the transport properties of symmetric alumina membrane [41], the asymmetric configuration with lower top layer thickness in the referenced works allow a higher flow, resulting in higher permeability even at lower open porosities.

Table 4
Comparison of water flux at 1 bar of transmembrane pressure in a dead-end configuration of alumina flat ceramic microfiltration membranes.

Preparation Method	Type	Open Porosity (%)	Average Pore Size (Top Layer) (µm)	Water Flux ($m^3\,m^{-2}\,h^{-1}$)	Reference
Pressing	Symmetric	43.1	0.350	0.165	Shaifei et al. (2013) [41]
Pressing/Tape Casting	Asymmetric	36.94	0.249	5.04	Zhu et al. (2019) [24]
Extrusion/ Slip Casting	Asymmetric	42	0.244	9.1	Terpstra et al. (1988) [40]
Freeze/Tape Casting	Asymmetric	43.69	0.32	28	this work
Freeze/Tape Casting	Asymmetric	37.39	0.36	32	this work
Freeze/Tape Casting	Asymmetric	26.16	0.35	11	this work

Furthermore, Table 4 allows a comparison according to the manufacturing process. Porous supports in which the pores were created by decomposing organic templates (e.g. from extruded or pressed samples) [40,24] show lower permeate flux than processes where the pore generation is more related to the nature of the solvent (e.g. phase inversion, freeze casting) [39, this work] especially due to the higher interconnectivity pores of those samples [39,42].

The combination of a freeze-cast support with a tape-cast layer to form an assembled asymmetric membrane, as carried out in this work, appears to be a promising manufacturing technique for microfiltration separation mainly due to the high water permeate flux. Moreover, this combination presents an easy porosity control and high interconnectivity obtained from the support together with the control of the thickness and pore distribution achieved for the separation layer.

4. Conclusions

In this work, assembled asymmetric alumina membranes with a separation layer were prepared by combining a porous support shaped by freeze casting and a separation cast tape layer. A highly porous structure with lamellar pores suitable for microfiltration can be achieved by freeze casting. SEM pictures show the morphology of both layers and the assembly of the structures without delamination.

Moreover, all membranes have presented a separation layer pore size in the microfiltration range ($< 0.4\,\mu m$). The mercury intrusion analysis suggests that the solvent plays a key role in the support porosity, while the separation layer is more affected by the binder content. Both layers do not show any significant changes in pore size distribution and average pore size in all condition tested. The pore size distribution of the assembled asymmetric membrane indicates that the structure is similar to the morphology of the porous support that has undergone two sintering steps.

The permeability results confirm that the separation layer rules the permeate flux mainly. The control of the morphology of the layers allowed the production of an asymmetric membrane with outstanding values of water permeate flux, which are the highest so far reported within the ranges of open porosity and pore size.

Declaration of Competing Interest

The authors declare that they have no known competing financial interests or personal relationships that could have appeared to influence the work reported in this paper.

Acknowledgments

Appendix A. Supplementary data

Supplementary material related to this article can be found, in the online version, at doi:https://doi.org/10.1016/j.jeurceramsoc.2020.07.069.

References

[1] R. Glimenius, Microfiltration- state of the art, Desalination 53 (1985) 363–372.
[2] C. Charcosset, Chapter 3 - microfiltration, Membrane Processes in Biotechnology and Pharmaceutics, Elsevier, New York, 2012.
[3] P. Luis, Chapter 1 - introduction, Fundamental Modelling of Membrane Systems, Elsevier, New York, 2018.
[4] M.M. Bazin, N. Ahmad, Y. Nakamura, Preparation of porous ceramic membranes from Sayong ball clay, J. Asian Ceram. Soc. 7 (4) (2019) 417–425.
[5] F. Bouzerara, A. Harabi, S. Condom, Porous ceramic membranes prepared from kaolin, Desalin. Water Treat. 12 (2009) 415–419.
[6] M.S.H. Bader, Seawater versus produced water in oil-fields water injection operations, Desalination 208 (2007) 159–168.
[7] M. Padaki, R. Surya Murali, M.S. Abdullah, N. Misdan, A. Moslehyani, M.A. Kassim, N. Hilal, A.F. Ismail, Membrane technology enhancement in oil-water separation. A review, Desalination 357 (2015) 197–207.
[8] R.J. Ciora Jr, P.K.T. Liu, Ceramic membranes for environmental related applications, Fluid/Particle Separation Journal 15 (1) (2003) 51–60.
[9] X. Tan, N. Liu, B. Meng, S. Liu, Morphology control of the perovskite hollow fibre membranes for oxygen separation using different bore fluids, J. Memb. Sci. 378 (2011) 308–318.
[10] P.L. Rachadel, J. Motuzas, R.A.F. Machado, D. Hotza, J.C. Diniz Da Costa, Influence of porous structures on O2 flux of BSCF asymmetric membranes, Sep. Purif. Technol. 175 (2017) 164–169.
[11] M.H.A. Aziz, M.H.D. Othman, N.A. Hashim, M.R. Adam, A. Mustafa, Fabrication and characterization of mullite ceramic hollow fiber membrane from natural occurring ball clay, Appl. Clay Sci. 177 (2019) 51–62.
[12] B.S. Benfer, P. Arki, G. Tomandl, Ceramic membranes for filtration applications-preparation and characterization, Adv. Eng. Mater. 6 (7) (2004) 495–500.
[13] C. Yang, G. Zhang, N. Xu, J. Shi, Preparation and application in oil - water separation of ZrO2/α-Al2O3 MF membrane, J. Memb. Sci. 142 (1998) 235–243.
[14] T. Fukasawa, Z.Y. Deng, M. Ando, Pore structure of porous ceramics synthesized from water-based slurry by freeze-dry process, J. Mater. Sci. 36 (2001) 2523–2527.
[15] Deville, S. Freeze-casting of porous ceramics: a review of current achievements and issues. Advanced Engineering Materials, 10, 3, p. 155–169.
[16] K.L. Scotti, D.C. Dunand, Freeze casting - a review of processing, microstructure and properties via the open data repository freezecasting.nEt, Prog. Mater. Sci. 94 (2018) 243–305.
[17] D.F. Souza, E.H.M. Nunes, J.A. Queiroga, W.L. Vasconcelos, Microstructural characterization and gas permeation performance of freeze-cast alumina supports, J. Eur. Ceram. Soc. 38 (11) (2018) 4020–4025.
[18] C. Gaudillere, J. Garcia-Fayos, M. Balaguer, J.M. Serra, Enhanced oxygen separation through robust freeze-cast bilayered dual-phase membranes, ChemSusChem 7 (2014) 2554–2561.
[19] H.-J. Yoon, U.-C. Kim, J.-H. Kim, Y.-H. Koh, Macroporous alumina ceramics with aligned microporous walls by unidirectionally freezing foamed aqueous ceramic suspensions, J. Am. Ceram. Soc. 93 (6) (2010) 1580–1582.
[20] S. Deville, E. Saiz, A.P. Tomsia, Ice-templated porous alumina structures, Acta Mater. 55 (2007) 1965–1974.
[21] R.K. Nishihora, P.L. Rachadel, M.G.N. Quadri, D. Hotza, Manufacturing porous ceramic materials by tape casting—a review, J. Eur. Ceram. Soc. 38 (4) (2018) 988–1001.
[22] D.M. Amaya, D. Estrada, D. Hotza, J.B. Rodrigues, J.A. Escobar, Porous Cu / YSZ anodes processed by aqueous tape casting for IT-SOFC, J. Eur. Ceram. Soc. 37 (16) (2017) 5233–5237.
[23] T.C.A. Silva, V.F. Kettermann, C. Pereira, M. Simoes, M. Wilhelm, K. Rezwan, Novel tape-cast SiOC-based porous ceramic electrode materials for potential application in bioelectrochemical systems, Journal of Material Science 54 (2019) 6471–6487.
[24] W. Zhu, Y. Liu, K. Guan, C. Peng, W. Qiu, J. Wu, Integrated preparation of alumina micro filtration membrane with super permeability and high selectivity, J. Eur. Ceram. Soc. 39 (4) (2019) 1316–1323.
[25] R.K. Nishihora, M.G.N. Quadri, D. Hotza, K. Rezwan, M. Wilhelm, Tape casting of polysiloxane-derived ceramic with controlled porosity and surface properties, J. Eur. Ceram. Soc. 38 (15) (2018) 4899–4905.
[26] L. Li, E. Gao, H. Abadikhah, J. Wang, L. Hao, X. Xu, S. Agathopoulos, Preparation of a porous, sintered membrane for filtration of an oil-in-water emulsion with high flux performance, Materials 11 (990) (2018) 1–15.
[27] D. Hotza, P.M. Geffroy, R.K. Nishihora, S. Bernard, Tape casting of preceramic polymers toward advanced ceramics: a review, Int. J. Ceramic Eng. Sci. 1 (2019) 21–41.
[28] D. Hotza, P. Greil, Review: aqueous tape casting of ceramic powders, Mater. Sci. Eng. A 202 (1995) 206–217.
[29] B.J. Bohnlein-Maus, W. Sigmund, G. Wegner, W.H. Meyer, F. Hesel, K. Seitz, A. Roosen, The function of polymers in the tape casting of alumina, Adv. Mater. 4 (2) (1992).
[30] P. Albano, L.B. Garrido, Influence of the slip composition on the properties of tape-cast alumina substrates, Ceram. Int. 31 (2005) 57–66.
[31] P. Monash, G. Pugazhenti, P. Saravan, Various fabrication methods of porous ceramic supports for membrane applications, Rev. Chem. Eng. 29 (5) (2013) 357–383.
[32] P.L. Rachadel, D.F. Souza, E.H.M. Nunes, J.C.D. Da Costa, W.L. Vasconcelos, D. Hotza, A novel route for manufacturing asymmetric BSCF-based perovskite structures by a combined tape and freeze casting method, J. Eur. Ceram. Soc. 37 (16) (2017) 5249–5257.
[33] C. Voigt, T. Zienert, P. Schubert, C.G. Aneziris, J. Hubalkova, Reticulated porous foam ceramics with different surface chemistries, J. Am. Ceram. Soc. 97 (7) (2014) 2046–2053.
[34] S.M. Miller, X. Xiao, J.A. Setlock, K.T. Faber, Freeze-cast alumina pore networks: effects of processing parameters in steady-state solidification regimes of aqueous slurries, J. Eur. Ceram. Soc. 38 (2018) 5134–5143.
[35] Z.W. Zhong, P. Arulvanan, C.F. Ang, Effects of sintering process conditions on size shrinkages of low-temperature co-fired ceramic substrate, Mater. Manuf. Process. 21 (2006) 721–726.

[36] A. Kalemtas, N. Ozey, M.T.A. Aydin, Processing of layered porous mullite ceramics, J. Aust. Ceram. Soc. 54 (3) (2018) 545–555.

[37] S.M. Samaei, S. Gato-Trinidad, A. Altaee, The application of pressure-driven ceramic membrane technology for the treatment of industrial wastewaters – a review, Sep. Purif. Technol. 200 (2018) 198–220.

[38] W. Zhou, L. Zhang, P. Wu, Y. Cai, X. Zhao, C. Yao, Study on permeability stability of sand-based microporous ceramic filter membrane, Materials 12 (2019) 1–14.

[39] R.K. Nishihora, E. Rudolph, M.G.N. Quadri, D. Hotza, K. Rezwan, M. Wilhelm, Asymmetric mullite membranes manufactured by phase-inversion tape casting from polymethylsiloxane and aluminum diacetate, J. Memb. Sci. 581 (2019) 421–429.

[40] R.A. Terpstra, B.C. Bonekamp, H.J. Veringa, Preparation, characterization and some properties of tubular alpha alumina ceramic membranes for microfiltration and as a support for ultrafiltration and gas separation membranes, Desalination 70 (1988) 395–404.

[41] K. Shafiei, M. Kazemimoghaddam, T. Mohammadi, S.G. Pakdehi, An investigation on manufacturing of alumina microfiltration membranes, Desalin. Water Treat. 53 (9) (2015) 2429–2436.

[42] X. Li, D. Yao, K. Zuo, Y. Xia, J. Yin, H. Liang, Y.-P. Zeng, Fabrication, microstructural characterization and gas permeability behavior of porous silicon nitride ceramics with controllable pore structures, J. Eur. Ceram. Soc. 39 (2019) 2855–2861.